Published in final edited form as:
Sci Signal. ; 7(335): ra69. doi:10.1126/scisignal.2005431.

The membrane protein Pannexin1 forms two open channel conformations depending on the mode of activation

Junjie Wang[1], **Cinzia Ambrosi**[2], **Feng Qiu**[1], **David G. Jackson**[1], **Gina Sosinsky**[2,3], and **Gerhard Dahl**[1,*]

[1]Department of Physiology and Biophysics, University of Miami, School of Medicine, Miami, Florida, 33136

[2]National Center for Microscopy and Imaging Research, Center for Research in Biological Systems

[3]Dept. of Neurosciences, University of California San Diego, La Jolla, CA, USA 92093-0608

Abstract

Pannexin1 (Panx1) participates in several signaling events that involve ATP release, including the innate immune response, ciliary beat in airway epithelia and oxygen supply in the vasculature. The view that Panx1 forms a large ATP-release channel has been challenged by the association of a low conductance, small anion-selective channel with the presence of Panx1. We showed that Panx1 membrane channels can function in two distinct modes with different conductances and permeabilities when heterologously expressed in *Xenopus* oocytes. When stimulated by potassium ions (K^+), Panx1 formed a high conductance channel of ~500 pS that was permeable to ATP. Various physiological stimuli can induce this ATP-permeable conformation of the channel in several cell types. In contrast, the channel had a low conductance (~50 pS) with no detectable ATP permeability when activated by voltage in the absence of K^+. The two channel states were associated with different reactivities of the terminal cysteine of Panx1 to thiol reagents, suggesting different conformations. Single particle electron microscopic analysis revealed that K^+ stimulated the formation of channels with a larger pore diameter than those formed in the absence of K^+. These data suggest that different stimuli lead to distinct channel structures with distinct biophysical properties.

Introduction

Pannexin1, 2, and 3 (Panx1, 2, 3) are a family of transmembrane proteins that oligomerize and form channels. Several independent lines of evidence have demonstrated that Panx1 forms the major ATP-release channel in many cell types. In *Xenopus* oocytes, Panx1 channels exhibited high permeability to ATP and mechanosensitivity (1). We previously showed that cells that released ATP through Panx1 channels included erythrocytes,

*Correspondence to: gdahl@miami.edu.

Author contributions: J.W. C.A., F.Q. and D.G.J. performed experiments, J.W., C.A., G.S and G.D. designed experiments, analyzed data and wrote the paper.

Competing interests: The authors declare no competing interests.

endothelial cells, astrocytes, airway epithelial cells, and stressed cardiac myocytes (2–5). ATP release colocalized with Panx1 channels in polarized cells, such as airway epithelia, where ATP is secreted exclusively at the air interface (4), or the apical membrane of kidney epithelial cells (6). Panx1 channels released ATP in the presence of increased intracellular cytoplasmic calcium (7) or in response to activation of purinergic receptors (7). These channels were permeable to cationic and anionic dyes that serve as surrogate measures for ATP release when taken up by cells from the extracellular medium (8–10). A direct correlation between ATP release and Panx1 abundance has also been reported (4, 11–13), as well as correlation between the pharmacology of the Panx1 channel, channel-mediated ATP release (14) and inhibition of Panx1 channels by extracellular ATP (9). Loss of the negative feedback inhibition by ATP resulted in increased ATP release (15). Finally, knocking out the function of Panx1 channels, which had been genetically engineered to have cysteines putatively located in the lining of the pore, by reaction with thiol reagents to block the pore also inhibited ATP release (16).

Despite this evidence for an ATP-release function of Panx1, two recent studies concluded that the Panx1 channel exhibited no ATP permeability (17, 18). These papers also reported a smaller unitary conductance of the Panx1 channel (~70 pS) than the 450 pS previously reported (1). The currents of the small conductance channel were attributed to fluxes of chloride ions (17, 18). This discrepancy could result from the properties of the Panx1 channel varying between cell types because of differing subunit compositions of the Panx (Panx1, 2, and 3) channels or by association of Panx1 with other proteins (18, 19). Other possible explanations include post-translational modifications that cause Panx1 to behave differently; the presence of auxiliary proteins that modify Panx1 channel properties; Panx1 modulating other channel proteins and not forming a channel itself; or the formation of distinct conductance and permeability states by the Panx1 channel that are activated by different stimuli.

The large conductance Panx1 channel was demonstrated in patch-clamping experiments in cells incubated with high concentrations of external potassium ions ($[K^+]_o$) (1, 2), stimulated to have increased cytoplasmic concentrations of calcium ions ($[Ca^{2+}]_i$) (7), exposed to mechanical stress (1), or placed in a low oxygen environment (20). All these conditions are associated with ATP release. Low oxygen conditions promote ATP release from erythrocytes, which is inhibited by Panx1 blockers (2, 21). Similarly, low oxygen activates the purinergic receptor P2Y2 in carotid body type II cells, which in turn stimulates ATP release for signal amplification, a process inhibited by Panx1 blockers (22). Mechanical (osmotic) stress induced ATP release from erythrocytes and airway epithelial cells, which was attenuated by either Panx1 knockdown or Panx1 blockers (4, 12). Similarly, ATP release induced by $[K^+]_o$ in oocytes and in astrocytes depended on the presence of Panx1 and was blocked by Panx1 inhibitors (1, 13, 23). In contrast, the low-conductance Panx1 channel was only observed in membrane patch-clamp experiments in response to voltage (positive membrane potential) in the presence of low extracellular K^+. Under these conditions, no ATP permeability was found. Instead, the Panx1 channel exhibited the properties of a small anion channel with high chloride permeability (17, 18). Because the different channel properties were observed under different experimental conditions, the formation of the two different conductance and permeability states is most likely due to

stimulus-specific phenomena rather than the other explanations considered above. We expressed Panx1 in *Xenopus* oocytes to test this hypothesis, because oocytes are well characterized and the paucity of endogenous channels minimizes the chance for erroneous attribution of channel properties. Additionally, Panx1 channels expressed in *Xenopus* oocytes exhibit voltage-dependent gating properties (1, 24), similar to those observed in other cell types, including neurons and astrocytes (19). In *Xenopus* oocytes, the Panx1 channel is closed at negative membrane potentials and requires membrane polarization to positive potentials to open. Yet, Panx1-mediated ATP release also occurs when cells or Panx1-expressing oocytes are exposed to high extracellular potassium ion concentration ($[K^+]_o$) (1, 2, 13). Elimination of the $[K^+]$ gradient across the plasma membrane reduces the membrane potential only to 0 mV and does not induce the positive potentials required to open Panx1. This apparent discrepancy is due to the allosteric activation of Panx1 channels by K^+, which is independent of membrane potential (23).

Results

Panx1-mediated ATP release is stimulus dependent

To test whether the two activation mechanisms (voltage and $[K^+]_o$) produce equivalent channel function, we used a luciferase assay to compare ATP release from *Xenopus* oocytes expressing Panx1 and control uninjected oocytes under voltage-clamp conditions (Fig. 1A). Clamping the membrane potential at +40 mV was ineffective in inducing ATP release, however, the addition of potassium gluconate to produce high $[K^+]_o$ stimulated ATP release from the Panx1-expressing oocytes. The low amount of ATP release from oocytes expressing Panx1 and held at +40 mV was similar to that observed in uninjected oocytes exposed to high $[K^+]_o$ or held at +40 mV. This low amount of ATP release is likely the result of fusion of ATP-containing vesicles with the plasma membrane, not channel activity (25). Membrane currents and ATP release did not correlate in uninjected oocytes or in oocytes expressing Panx1 held at +40 mV under voltage-clamp condition (Fig. 1B). The wide range of currents observed for the injected oocytes was indicative of the different amounts of Panx1 expressed by each oocyte and clearly showed that ATP release occurred independently of the current. In uninjected oocytes, the membrane currents were small and homogeneous, and ATP release varied over the same range as in the Panx1-expressing oocytes. Carbenoxolone (CBX) is a Panx1 inhibitor that attenuates both voltage-induced Panx1 currents, as well as K^+-induced ATP release from cells (2, 26). At higher concentrations CBX also inhibits connexin gap junction and hemichannels (26). ATP release at +40 mV was similar in the presence or absence of CBX (Fig. 1C), suggesting that Panx1 channels did not mediate the small amount of ATP released at +40 mV in Panx1-expressing oocytes, despite robust clamp currents indicating channel opening (Fig. 1D).

Under voltage-clamp conditions, 150 mM $[K^+]_o$ stimulated ATP release independently of the holding potential (Fig. 1C). Even with the membrane potential clamped to −60 mV, $[K^+]_o$ led to a similar amount of ATP release as that from unclamped oocytes (Fig. 1C). Clamping the membrane potential at 0 or +40 mV did not further increase ATP release stimulated by $[K^+]_o$.

Because caspase cleavage of the Panx1 C-terminus has been reported as an activation mechanism for ATP release (27), we tested the properties of K^+-stimulated channel function. Extracellular K^+ stimulated ATP release from non-voltage-clamped oocytes expressing Panx1 in a dose-dependent manner (Fig. 2A) and was prominent at $[K^+]_o$ as low as 20 mM. Reducing $[K^+]_o$ to 1 mM following stimulation with 150 mM $[K^+]_o$, eliminated ATP release (Fig. 2B), indicating that stimulation by K^+ was reversible and ruling out activation by caspase cleavage of C-terminal moieties of Panx1.

Connexin 46-mediated ATP release is inducible by voltage

To test whether stimulus-mode specific ATP release is particular to Panx1 channels, we tested another large-conductance channel permeable to ATP. Connexin channels typically form gap junctions between cells. Certain connexins, including Connexin46 (Cx46), can form unpaired membrane channels (referred to as hemichannels) in low extracellular calcium concentrations (28). In 1 mM $[Ca^{2+}]_o$, Cx46 channels open in response to depolarization.. Gap junction channels and hemichannels are permeable to ATP (29). Cx46-expressing oocytes released ATP when the membrane potential was clamped at 0 mV, and this release was blocked by 200 μM CBX (Fig. 2C). Thus, Cx46 hemichannels released ATP in response to voltage stimulation alone unlike Panx1 channels, which under identical experimental conditions did not release ATP (Fig. 1C).

Single-channel properties vary with different activation mechanisms

Next, we tested the hypothesis that the two permeability states of Panx1 channels correlate with the two conductance states of the channel (1, 17). Analysis of the experimental conditions used in these previous studies hinted at different extracellular ionic conditions as responsible for the difference in channel properties. To determine whether the extracellular ion composition affects single-channel conductance, we analyzed Panx1-expressing oocytes by patch clamp. As reported previously (1), with 150 mM $[K^+]_o$, the Panx1 channel is active over a wide voltage range, exhibits multiple subconductance states, and the maximal single channel conductance (g_{max}) is ~500 pS. In the present study, when held at −100 mV in 150 mM $[K^+]_o$ we observed a maximal single-channel conductance of 520 ± 37 pS (n=4) (Fig. 3A). Under this condition, the fully open and the fully closed states were rare and brief events and the channel mainly dwelled in various subconductance states in concordance with previous reports (1, 7, 30). With regular Ringer solution outside (80 mM Na^+ and 1 mM K^+), channel activity was only observed at positive potentials, the unitary conductance was 44 ± 4 pS (n=4), and no subconductances were observed (Fig. 3B). The reversibility of the Panx1 large-conductance channel activity was clearly visible by changing the ionic composition of the perfusate of an outside-out membrane patch from K^+ to Na^+ and back (Fig. 3C).

Reactivity of C-terminal cysteine is stimulus dependent

Previously, using the substituted cysteine accessibility method (SCAM) to determine pore-lining amino acids in the voltage-activated Panx1 channel (16), we found that the C-terminal cysteine of Panx1, as well as amino acids adjacent to that had been replaced by cysteine, were reactive to thiol reagents when the channel was opened by stepping the membrane potential to positive potentials. Because the structure of the channel could be different when

activated by different stimuli, we tested whether thiol reagents modify K^+-induced Panx1 currents. Maleimidobutyrylbiocitin (MBB) is a 565-Da thiol reagent that irreversible modifies cysteines and has the potential to partially obstruct the permeation pathway if the reactive cysteine is located in or close to the pore (16).

We measured Panx1 currents stimulated by K^+ or voltage in the presence and absence of MBB. The K^+-activated Panx1 channel current was not inhibited by MBB (Fig. 4A). In contrast, MBB inhibited the voltage-activated Panx1 current in the same cell following washout of K^+ (Fig. 4B), consistent with a previous report (16). We also tested the methanethiosulfonate, MTSET, which is 278 Da and reacts reversibly with thiol groups. MTSET application to oocytes expressing wild-type Panx1 activated by K^+ did not attenuate the channel conductance (1.7±1.6% inhibition, n=4) (Fig. 4E). The lack of inhibition of channel conductance by both MBB and MTSET suggests that the C-terminal cysteine is not accessible to the thiol reagents in the K^+-gated channel configuration, but becomes accessible in the voltage-gated configuration.

Our previous SCAM analysis also identified amino acids at the transition between the first transmembrane segment and the first extracellular loop as potentially pore-lining moieties (16). We tested one of these cysteine mutants ($Panx1^{T62C,\ C426S}$) for reactivity to thiol reagents. In contrast to the C-terminal cysteine of wild-type Panx1, the $Panx1^{T62C,C426S}$ mutant reacted with thiol reagents in the K^+-activated state and the voltage-activated state, the latter was shown previously for both MTSET and MBB (16). These data suggest that K^+ mainly alters the arrangement of the C-terminal moieties, while the configuration of the pore lining at the extracellular vestibulum may be similar for both voltage- and K^+-activated Panx1 channels.

Electron microscopic (EM) analysis of the pore diameter of Panx1 channels under two conditions reveals stimulus-dependent size differences

Because Panx1 channels can be differentially activated by extracellular K^+, we could study the structure of both the activated and the inactivated channels in solution. Using Panx1 channels purified from baculovirus-infected Sf9 cells (31) (Fig. 5A), we performed negative stain low dose EM imaging of Panx1 channels diluted 1:14 with either water (unstimulated condition) or 50 mM KCl (stimulated condition). We identified structures with two different pore sizes (Fig. 5B, C). The heterogeneous appearance of the Panx1 channels is due to different orientations of the particles as they lay onto the grid. Two types of Panx1 channels, with distinct pore staining, but similar channel sizes, are clearly visible in these EM micrographs (Fig. 5B, C) and represent Panx1 channels in different orientations. In particular, we analyzed the orientations in which (i) the cytoplasmic surfaces faced toward the EM vacuum (extracellular surface faced the grid) or (ii) the extracellular surface faced up (cytoplasmic surface faced the grid). We assigned these views on the basis of the pannexin channels having a similar quaternary architecture as connexin channels with monomers larger than 40 kD (28) and cytoplasmic versus extracellular channel diameters measured in the Cx26 dodecameric X-ray atomic model (32)

From several micrographs, we selected 500 Panx1 channels from the unstimulated condition (no KCl added) and 600 from the K^+-stimulated condition. We used EMAN2 class

averaging procedures to classify the different channel orientations for subsequent image averaging. Within these class averages (subsets of the 500 or 600 particle images), we then measured the diameters of the channel and the pore for units that showed distinct staining within the pores to mitigate the effects of slight tilts on these face views (Fig. 5D). Typically, 4–5 class averages for each orientation showed distinctly stained central pores. Because Panx1 forms hexameric channels (31, 33), we also displayed a hexagonally symmetrized class average. One class average from each condition is depicted in Fig. 5D. We measured diameters on unsymmetrized class averages. We found little significant difference between the Panx1 channel diameters (~160–170 Å for cytoplasmic surface views and ~108 Å for extracellular surface views), but an over 300% increase in pore diameters (~54 vs. ~15 Å) at the cytoplasmic surface and a 29% (~44 vs. ~34 Å) at the extracellular surface for Panx1 channels incubated in 50 mM KCl (see distributions of measurements plot from the class averages in Fig. 5E). These structural data further substantiate the results of the electrophysiological experiments, establishing the formation of two distinct channels with different pore characteristics that depend on the activation mechanism.

Discussion

On the basis of the data we have presented, we propose that Panx1 channels can exhibit distinct and unique conductances and permeabilities in the same cellular environment with only the stimulation modus as the variable. We observed these two channel properties in the same Panx1-expressing oocytes, but under two different activation conditions. Hence, it is unlikely that other proteins modulate Panx1 in order to assume different conductances and permeabilities, as has been previously suggested (17, 18). Instead, it appears that Panx1 itself can assume two distinct channel conformations and that the mode of activation determines the configuration.

The high-conductance and large-pore configuration of the Panx1 channel likely predominates in most physiological and pathological settings. Many physiological stimuli open the Panx1 channel in cells at the resting membrane potential (Table 1), where both concentration gradient for ATP and electrical gradient are directed outwards and thus support efficient ATP release. Voltage gating, on the other hand, is an unlikely stimulus in vivo. The very high positive voltage required to open Panx1 channels is a rare event only associated with cells that form action potentials. A limited number of cell types, including neurons and muscle cells, exhibit action potentials for their functionality and, with the exception of heart muscle, these are of very brief duration, lasting about a millisecond. Not surprisingly, membrane potential–induced ATP release from nerve terminals is mainly, if not exclusively, vesicular in nature (34–37). The positive potentials required for Panx1 channel activation approximate the reversal potential for $MgATP^{2-}$ and ATP^{4-}. Indeed, as indicated in a recent study of connexin hemichannels (38), a membrane potential of +80 mV is close to or even beyond the reversal potential for ATP. ATP flux through connexin hemichannels, which only open at extreme positive potentials, did not occur while the membrane potential was stepped to +80 mV. Instead, a brief ATP release was associated with the tail currents after stepping the membrane potential back to −40 mV. Although tail currents are useful analysis tools, they are experimental artifacts. In vivo, membrane channels do not operate under voltage-clamp conditions. A cell would need a combination

of slowly-inactivating depolarizing channels combined with fast-opening hyperpolarizing channels to approximate the situation encountered experimentally in tail currents. However, most ATP release in vivo occurs at the resting membrane potential or in slightly depolarized cells, conditions in which connexin hemichannels are closed and Panx1 channels are activated by other means than changes in membrane voltage.

Physiological stimuli for Panx1 typically induce the large conductance configuration. These stimuli include low oxygen, mechanical stress caused by hypotonic conditions, increased cytoplasmic calcium concentration, and ATP and glutamate signaling through their cognizant receptors (7, 39) (Table 1). Oxygen deprivation from erythrocytes or neurons induces the high conductance channel configuration with permeability to ATP and similarly sized molecules (2, 20). Similarly, increased calcium ion concentration activates a 500-pS channel in oocytes expressing Panx1. ATP and glutamate activate the large Panx1 channel configuration in oocytes coexpressing Panx1 with purinergic receptors (7, 8) and in neurons through activation of the NMDA receptor (39), respectively. Because the properties of the K^+-activated channel appear to mimic those of the Panx1 channel activated by the physiological stimuli listed above, K^+ can be used as a surrogate for the physiological stimuli.

The stimulus used in the present study, extracellular K^+, is required at concentrations considerably higher than the normal extracellular $[K^+]$, which is tightly controlled and varies only minimally. For example, in the central nervous system, the $[K^+]_o$ is low and undergoes minor variations in response to neuronal activity (40). However, after middle cerebral artery occlusion, $[K^+]_o$ in the core of the lesion increases to >50 mM and progressively decreases in the penumbra (41, 42). Similarly high $[K^+]_o$ has been observed during spreading depression in the cerebral cortex (40). A moderate increase of $[K^+]_o$ to ~10 mM has been observed during epileptiform convulsions (40) and such small $[K^+]_o$ increases activate Panx1 in astrocytes (13).

Thus, under pathological conditions, high $[K^+]_o$ is a realistic stimulus for the Panx1 channel. Under pathological conditions, K^+ is not only an allosteric stimulus for Panx1 but also attenuates the feedback inhibition of the channel by ATP (43). Under physiological conditions, this feedback inhibition prevents unlimited amplification of the ATP signal in cells coexpressing Panx1 with purinergic receptors capable of activating Panx1 (7–9). Thus, a combination of ATP and extracellular $[K^+]$ increase puts cells at high risk for inflammatory cell death (43).

The present study shows that the exclusively voltage-gated Panx1 channel when expressed in oocytes is impermeable to ATP. This observation is consistent with the findings by Ma *et al*. (16) and Romanov *et al*. (17), who used other cellular expression systems. This, however, does not preclude voltage- induced ATP release through Panx1 channels by indirect mechanisms. For example, voltage-gated calcium channels could result in Ca^{2+} influx, which in turn activates Panx1. Alternatively, voltage-activated mechanisms could lead to posttranslational modification of Panx1 and thereby activate the large pore channel. Activation of the large pore conformation under voltage conditions that would otherwise promote the small conductance, small pore conformation are possible, because, as shown in

Figs. 1 and 3, alternative activation mechanisms, such as K^+ stimulation, can overrride the voltage gate for determining the channel configuration. The small channel conformation of Panx1 may serve a specific physiological function as yet not recognized. Just as K^+ is a surrogate activation mechanism of the "large" Panx1 channel conformation, the voltage activation may mimic an as yet to be identified physiological stimulus for the "small" Panx1 channel.

The observation that different stimuli can induce different conformations of a membrane channel with distinct conductances and permeabilities is unusual. To our knowledge, only one channel, the ligand-operated purinergic receptor $P2X_7R$, has been associated with a similar phenomenon. Depending on ligand application, brief versus long or single versus repetitive exposure to ATP, $P2X_7R$ is a small, cation-selective channel or a large pore with no selectivity except a size exclusion limit of <1 kD. However, the nature of this "pore dilation" of $P2X_7R$ is presently controversial and the possibility that Panx1 or other proteins represent the large pore conductance reported for $P2X_7R$ remains an option (8, 10, 44, 45).

Materials and Methods

All procedures were conducted in accordance with the Guiding Principles for Research Involving Animals and Human Beings of American Physiological Society. Ovaries were harvested from adult female *Xenopus laevis.* Ovaries were cut into small pieces and incubated in 2.5 mg/ml of collagenase (Worthington) calcium-free oocyte Ringer (OR) solution, stirring at one turn/second at room temperature. Typically, the incubation period was 3 h for oocytes to be separated from the follicle cells.

The plasmid containing mouse Panx1 in pCS2 was linearized with Not I. In vitro transcription were performed with polymerases SP6, using the Message Machine kit (Ambion, Austin, TX). mRNAs were quantified by absorbance (260 nm), and the proportion of full-length transcripts was checked by agarose gel electrophoresis. In vitro transcribed mRNAs (40 nl) were injected into *Xenopus* oocytes. Cells were kept in regular Ringer solution OR (82.5 mM NaCl, 2.5 mM KCl, 1 mM Na_2HPO_4, 1 mM $MgCl_2$, 1mM $CaCl_2$ and 5 mM HEPES) with 10 mg/ml antibiotics streptomycin.

Whole-cell membrane currents of oocytes were measured using a two-electrode voltage clamp (Gene Clamp 500B, Axon Instruments/Molecular Devices Sunnyvale, CA USA). Glass pipettes were pulled using a P-97 Flaming/Brown type puller (Sutter, Novato, USA). For thiol reaction of the native C426 of Panx1 and the engineered $Panx1^{T62C,\ C426S}$ MBB (from Calbiochem) was initially used. However, MBB presently is not further available, hence the switch to MTSET (from Toronto Research Chemicals), which yielded similar results as MBB in our previous SCAM analysis (16).

Single Panx1 channel activity was studied with the patch-clamp technique using a WPC 100 amplifier (E.S.F. Electronic, Goettingen, Germany). The oocytes' vitelline membranes were manually removed by forceps. For inside-out patches, both the bath and pipette solutions contained 140 mM KGlu, 10 mM KCl, and 5 mM TES, pH 7.5. For outside-out patches,

both the pipette and bath solutions contained 140 mM NaCl, 10 mM KCl, and 5 mM TES, pH 7.5.

ATP release was determined by luminometry. To open Panx1 channels, oocytes were either exposed to solutions with increased potassium ion concentration or the membrane potential was held at positive voltages through a voltage clamp circuit. Unless otherwise noted, after 20 minutes of stimulation an aliquot of the supernatant (50 μl) was collected and assayed with luciferase/luciferin (Promega, Madison, USA).

For electron microscopic structure analysis, Panx1 hemichannels were isolated from baculovirus-infected Sf9 cells according to published methods using a His^6 tag affinity purification protocol (31, 46, 47). Specimens were assessed for purity using SDS PAGE and Western blots (31, 48). A solution of about 2.8 mg/ml of purified Panx1, in elution buffer, was diluted in double distilled water (unstimulated condition) or in 50 mM KCl (stimulated condition). The diluted sample was adsorbed on carbon-coated grids and negative stained using 2% uranyl acetate. After blotting, the grids were imaged on a FEI Technai Spirit (Hillsboro, OR) operated at 120 keV. Low dose images were collected using Serial EM software (49) and a TVIPS TemCam-F224 2k × 2k CCD camera (TVIPS, Gauting, Germany). Images were acquired at 30 kX magnification with a 1.6 post-column magnification and had an effective pixel step size of 4.2 Å/pixel on the specimen. The dose on the specimen was in the range of 4–8 $e^{-}/Å^2$. Class averages and C6 symmetrized averages were performed using EMAN2 (48). The diameter measurements in Fig. 5D represent “an average of averages” because the total numbers of images used in computing cytoplasmic and extracellular surface views averages ranged between 46 and 78 images per surface view for the unstimulated and 50 mM KCl-stimulated conditions, respectively.

Acknowledgments

We thank S. Locovei for some of the single channel records and S. Phan for his assistance with the low dose electron microscopy.

Funding: Supported by the Craig Nielsen Foundation (GD), NIH grants GM065937 (GES) and GM072881 (GES). The National Center for Microscopy and Imaging Research is supported by GM103412 (Mark H. Ellisman).

References and Notes

1. Bao L, Locovei S, Dahl G. Pannexin membrane channels are mechanosensitive conduits for ATP. FEBS Lett. 2004; 572:65–68. [PubMed: 15304325]
2. Locovei S, Bao L, Dahl G. Pannexin 1 in erythrocytes: Function without a gap. Proc Natl Acad Sci U S A. 2006; 103:7655–7659. [PubMed: 16682648]
3. Iglesias R, Dahl G, Qiu F, Spray DC, Scemes E. Pannexin 1: the molecular substrate of astrocyte "hemichannels". J Neurosci. 2009; 29:7092–7097. [PubMed: 19474335]
4. Ransford GA, Fregien N, Qiu F, Dahl G, Conner GE, Salathe M. Pannexin 1 contributes to ATP release in airway epithelia. Am J Respir Cell Mol Biol. 2009; 41:525–534. [PubMed: 19213873]
5. Dolmatova E, Spagnol G, Boassa D, Baum JR, Keith K, Ambrosi C, Kontaridis MI, Sorgen PL, Sosinsky GE, Duffy HS. Cardiomyocyte ATP release through pannexin 1 aids in early fibroblast activation. Am J Physiol Heart Circ Physiol. 2012; 303:H1208–H1218. [PubMed: 22982782]
6. Hanner F, Lam L, Nguyen MT, Yu A, Peti-Peterdi J. Intrarenal localization of the plasma membrane ATP channel pannexin1. Am J Physiol Renal Physiol. 2012; 303:F1454–F1459. [PubMed: 22952282]

7. Locovei S, Wang J, Dahl G. Activation of pannexin 1 channels by ATP through P2Y receptors and by cytoplasmic calcium. FEBS Lett. 2006; 580:239–244. [PubMed: 16364313]
8. Locovei S, Scemes E, Qiu F, Spray DC, Dahl G. Pannexin1 is part of the pore forming unit of the P2X(7) receptor death complex. FEBS Lett. 2007; 581:483–488. [PubMed: 17240370]
9. Qiu F, Dahl G. A permeant regulating its permeation pore: inhibition of pannexin 1 channels by ATP. Am J Physiol Cell Physiol. 2009; 296:C250–C255. [PubMed: 18945939]
10. Pelegrin P, Surprenant A. Pannexin-1 mediates large pore formation and interleukin-1beta release by the ATP-gated P2X7 receptor. EMBO J. 2006; 25:5071–5082. [PubMed: 17036048]
11. Qu Y, Misaghi S, Newton K, Gilmour LL, Louie S, Cupp JE, Dubyak GR, Hackos D, Dixit VM. Pannexin-1 Is Required for ATP Release during Apoptosis but Not for Inflammasome Activation. J Immunol. 2011; 186:6553–6561. [PubMed: 21508259]
12. Qiu F, Wang J, Spray DC, Scemes E, Dahl G. Two non-vesicular ATP release pathways in the mouse erythrocyte membrane. FEBS Lett. 2011; 585:3430–3435. [PubMed: 21983290]
13. Suadicani SO, Iglesias R, Wang J, Dahl G, Spray DC, Scemes E. ATP signaling is deficient in cultured pannexin1-null mouse astrocytes. Glia. 2012; 60:1106–1116. [PubMed: 22499153]
14. Dahl G, Qiu F, Wang J. The bizarre pharmacology of the ATP release channel pannexin1. Neuropharmacology. 2013
15. Qiu F, Wang J, Dahl G. Alanine substitution scanning of pannexin1 reveals amino acid residues mediating ATP sensitivity. Purinergic Signal. 2012; 8:81–90. [PubMed: 21987098]
16. Wang J, Dahl G. SCAM analysis of Panx1 suggests a peculiar pore structure. J Gen Physiol. 2010; 136:515–527. [PubMed: 20937692]
17. Ma W, Compan V, Zheng W, Martin E, North RA, Verkhratsky A, Surprenant A. Pannexin 1 forms an anion-selective channel. Pflugers Arch. 2012; 463:585–592. [PubMed: 22311122]
18. Romanov RA, Bystrova MF, Rogachevskaya OA, Sadovnikov VB, Shestopalov VI, Kolesnikov SS. The ATP permeability of pannexin 1 channels in a heterologous system and in mammalian taste cells is dispensable. J Cell Sci. 2012; 125:5514–5523. [PubMed: 22956545]
19. MacVicar BA, Thompson RJ. Non-junction functions of pannexin-1 channels. Trends Neurosci. 2010; 33:93–102. [PubMed: 20022389]
20. Thompson RJ, Zhou N, MacVicar BA. Ischemia opens neuronal gap junction hemichannels. Science. 2006; 312:924–927. [PubMed: 16690868]
21. Sridharan M, Adderley SP, Bowles EA, Egan TM, Stephenson AH, Ellsworth ML, Sprague RS. Pannexin 1 is the conduit for low oxygen tension-induced ATP release from human erythrocytes. Am J Physiol Heart Circ Physiol. 2010; 299:H1146–H1152. [PubMed: 20622111]
22. Zhang M, Piskuric NA, Vollmer C, Nurse CA. P2Y2 receptor activation opens pannexin-1 channels in rat carotid body type II cells: potential role in amplifying the neurotransmitter ATP. J Physiol. 2012; 590:4335–4350. [PubMed: 22733659]
23. Silverman WR, de Rivero Vaccari JP, Locovei S, Qiu F, Carlsson SK, Scemes E, Keane RW, Dahl G. The pannexin 1 channel activates the inflammasome in neurons and astrocytes. J Biol Chem. 2009; 284:18143–18151. [PubMed: 19416975]
24. Bruzzone R, Hormuzdi SG, Barbe MT, Herb A, Monyer H. Pannexins, a family of gap junction proteins expressed in brain. Proc Natl Acad Sci U S A. 2003; 100:13644–13649. [PubMed: 14597722]
25. Maroto R, Hamill OP. Brefeldin A block of integrin-dependent mechanosensitive ATP release from Xenopus oocytes reveals a novel mechanism of mechanotransduction. J Biol Chem. 2001; 276:23867–23872. [PubMed: 11320093]
26. Bruzzone R, Barbe MT, Jakob NJ, Monyer H. Pharmacological properties of homomeric and heteromeric pannexin hemichannels expressed in Xenopus oocytes. J Neurochem. 2005; 92:1033–1043. [PubMed: 15715654]
27. Chekeni FB, Elliott MR, Sandilos JK, Walk SF, Kinchen JM, Lazarowski ER, Armstrong AJ, Penuela S, Laird DW, Salvesen GS, Isakson BE, Bayliss DA, Ravichandran KS. Pannexin 1 channels mediate 'find-me' signal release and membrane permeability during apoptosis. Nature. 2010; 467:863–867. [PubMed: 20944749]

28. Paul DL, Ebihara L, Takemoto LJ, Swenson KI, Goodenough DA. Connexin46, a novel lens gap junction protein, induces voltage-gated currents in nonjunctional plasma membrane of Xenopus oocytes. Journal of Cell Biology. 1991; 115:1077–1089. [PubMed: 1659572]
29. Harris AL. Connexin channel permeability to cytoplasmic molecules. Prog Biophys Mol Biol. 2007; 94:120–143. [PubMed: 17470375]
30. Dahl G, Locovei S. Pannexin: To Gap or not to Gap, is that a question? IUBMB Life. 2006; 58:409–419. [PubMed: 16801216]
31. Ambrosi C, Gassmann O, Pranskevich JN, Boassa D, Smock A, Wang J, Dahl G, Steinem C, Sosinsky GE. Pannexin1 and Pannexin2 channels show quaternary similarities to connexons and different oligomerization numbers from each other. J Biol Chem. 2010; 285:24420–24431. [PubMed: 20516070]
32. Maeda S, Nakagawa S, Suga M, Yamashita E, Oshima A, Fujiyoshi Y, Tsukihara T. Structure of the connexin 26 gap junction channel at 3.5 A resolution. Nature. 2009; 458:597–602. [PubMed: 19340074]
33. Boassa D, Ambrosi C, Qiu F, Dahl G, Gaietta G, Sosinsky G. Pannexin1 channels contain a glycosylation site that targets the hexamer to the plasma membrane. J Biol Chem. 2007; 282:31733–31743. [PubMed: 17715132]
34. Silinsky EM. On the association between transmitter secretion and the release of adenine nucleotides from mammalian motor nerve terminals. J Physiol. 1975; 247:145–162. [PubMed: 166162]
35. Wagner JA, Carlson SS, Kelly RB. Chemical and physical characterization of cholinergic synaptic vesicles. Biochemistry. 1978; 17:1199–1206. [PubMed: 656382]
36. MacKenzie I, Burnstock G, Dolly JO. The effects of purified botulinum neurotoxin type A on cholinergic, adrenergic and non-adrenergic, atropine-resistant autonomic neuromuscular transmission. Neuroscience. 1982; 7:997–1006. [PubMed: 6124898]
37. Unsworth CD, Johnson RG. Acetylcholine and ATP are coreleased from the electromotor nerve terminals of Narcine brasiliensis by an exocytotic mechanism. Proc Natl Acad Sci U S A. 1990; 87:553–557. [PubMed: 2137245]
38. Nualart-Marti A, del Molino EM, Grandes X, Bahima L, Martin-Satue M, Puchal R, Fasciani I, Gonzalez-Nieto D, Ziganshin B, Llobet A, Barrio LC, Solsona C. Role of connexin 32 hemichannels in the release of ATP from peripheral nerves. Glia. 2013; 61:1976–1989. [PubMed: 24123415]
39. Thompson RJ, Jackson MF, Olah ME, Rungta RL, Hines DJ, Beazely MA, MacDonald JF, MacVicar BA. Activation of pannexin-1 hemichannels augments aberrant bursting in the hippocampus. Science. 2008; 322:1555–1559. [PubMed: 19056988]
40. Somjen GG. Extracellular potassium in the mammalian central nervous system. Annu Rev Physiol. 1979; 41:159–177. [PubMed: 373587]
41. Gido G, Kristian T, Siesjo BK. Extracellular potassium in a neocortical core area after transient focal ischemia. Stroke. 1997; 28:206–210. [PubMed: 8996513]
42. Sick TJ, Feng ZC, Rosenthal M. Spatial stability of extracellular potassium ion and blood flow distribution in rat cerebral cortex after permanent middle cerebral artery occlusion. J Cereb Blood Flow Metab. 1998; 18:1114–1120. [PubMed: 9778188]
43. Jackson DG, Wang J, Keane RW, Scemes E, Dahl G. ATP and potassium ions: a deadly combination for astrocytes. Sci Rep. 2014; 4:4576. [PubMed: 24694658]
44. Browne LE, Compan V, Bragg L, North RA. P2X7 receptor channels allow direct permeation of nanometer-sized dyes. J Neurosci. 2013; 33:3557–3566. [PubMed: 23426683]
45. Suadicani SO, Iglesias R, Spray DC, Scemes E. Point mutation in the mouse P2X7 receptor affects intercellular calcium waves in astrocytes. ASN Neuro. 2009; 1
46. Oshima A, Tani K, Hiroaki Y, Fujiyoshi Y, Sosinsky GE. Three-dimensional structure of a human connexin26 gap junction channel reveals a plug in the vestibule. Proc Natl Acad Sci U S A. 2007; 104:10034–10039. [PubMed: 17551008]
47. Ambrosi C, Boassa D, Pranskevich J, Smock A, Oshima A, Xu J, Nicholson BJ, Sosinsky GE. Analysis of four connexin26 mutant gap junctions and hemichannels reveals variations in hexamer stability. Biophys J. 2010; 98:1809–1819. [PubMed: 20441744]

48. Tang G, Peng L, Baldwin PR, Mann DS, Jiang W, Rees I, Ludtke SJ. EMAN2: an extensible image processing suite for electron microscopy. J Struct Biol. 2007; 157:38–46. [PubMed: 16859925]

49. Mastronarde DN. Automated electron microscope tomography using robust prediction of specimen movements. J Struct Biol. 2005; 152:36–51. [PubMed: 16182563]

50. Silverman W, Locovei S, Dahl G. Probenecid, a gout remedy, inhibits pannexin 1 channels. Am J Physiol Cell Physiol. 2008; 295:C761–C767. [PubMed: 18596212]

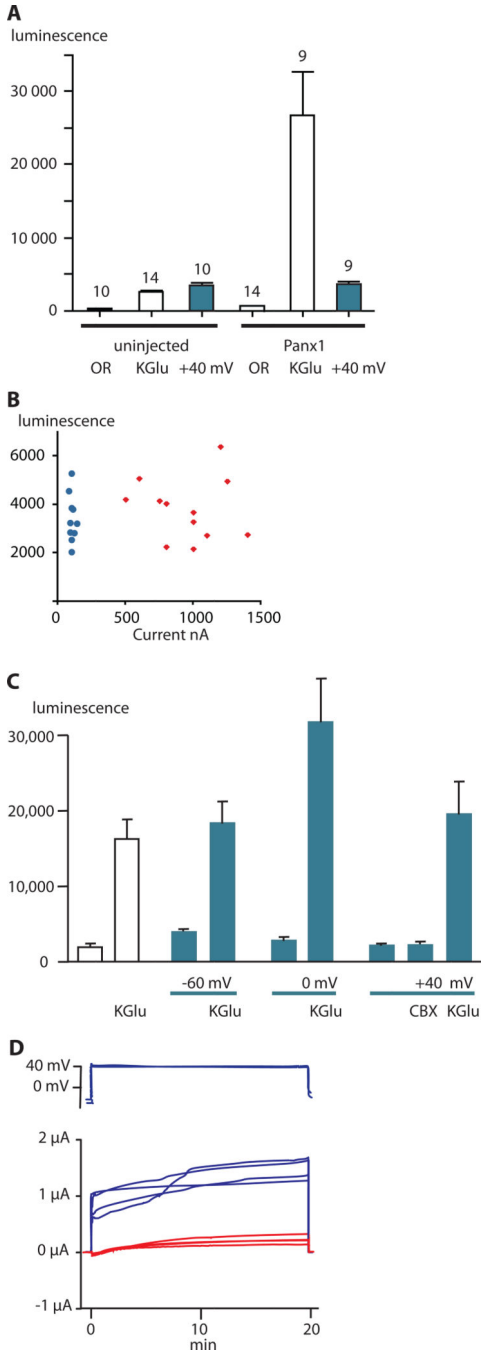

Fig. 1.

ATP release from uninjected and Panx1-expressing oocytes. All colored bars represent data obtained under voltage-clamp conditions; white bars are data from unclamped cells. ATP in the media was measured as luciferase luminescence.**(A)** ATP release from uninjected oocytes or Panx1-expressing oocytes in the presence of oocyte Ringer solution (OR), 150 mM potassium gluconate (KGlu) solution, or to holding the membrane potential at +40 mV under voltage-clamp conditions. Data are shown as means ± SD. N is indicated above the bars.

(B) Membrane currents and ATP release in uninjected and Panx1-expressing oocytes with the membrane potential held at +40 mV. Blue = uninjected and red = Panx1-injected oocytes.

(C) ATP release from Panx1-expressing oocytes induced by KGlu with and without holding the membrane potential under voltage-clamp conditions at −60, 0, or +40 mV. Voltage-clamp conditions are indicated with blue lines below the graph and blue bars in the graph. Open bars are data from oocytes that were not voltage clamped. The presence of 150 mM KGlu or 100 μM carbenoxolone (CBX) is indicated. Data are shown as means ± SD. N=5 for each measurement.

(D) Membrane currents of oocytes used in experiments shown in C. The voltage traces (top) start with the resting potential followed by the holding potential at +40 mV. Blue current traces: membrane potential stepped from the resting membrane potential to +40 mV. Red current traces: membrane potential stepped from the resting membrane potential to 0 mV in the presence of 150 mM KGlu.

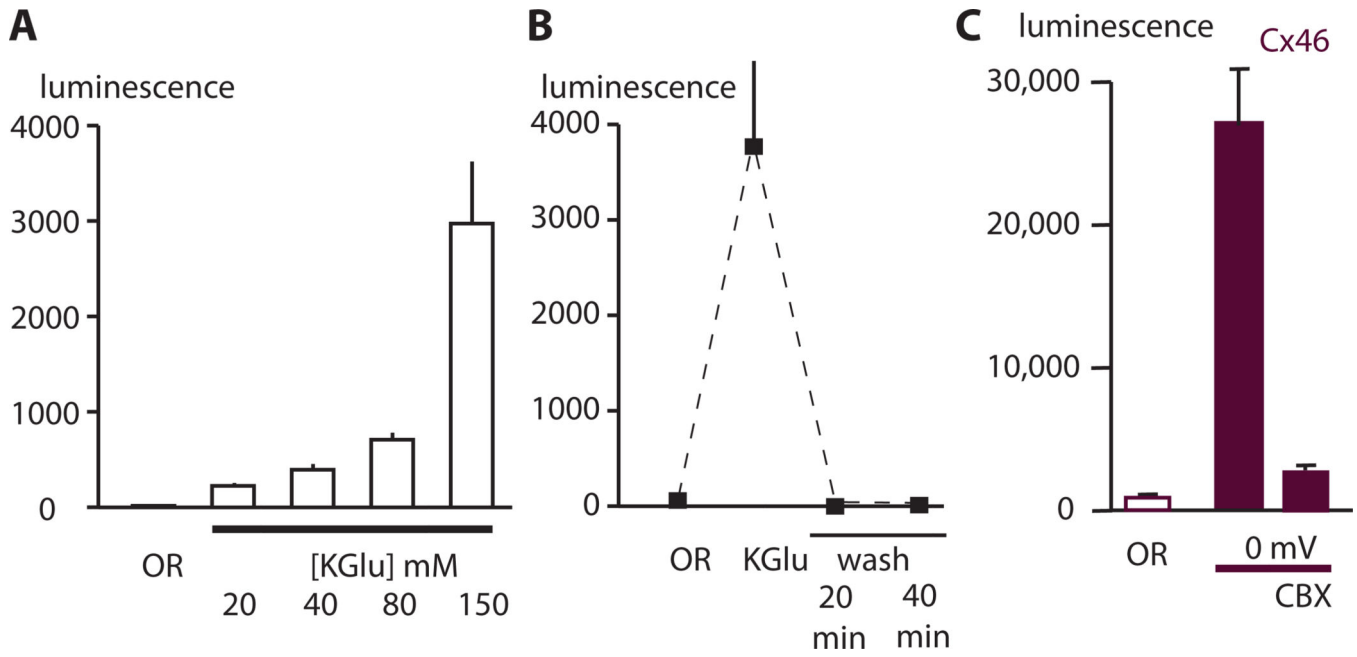

Fig. 2.

K^+-induced ATP release from Panx1-expressing oocytes. **(A)** Dose-dependent induction of ATP release from Panx1-expressing oocytes. Panx1-expressing oocytes were exposed for 20 minutes to Ringer solutions with increased K^+ (replacing Na^+) and aliquots of the supernatant were collected for ATP measurements with the luciferase assay.. **(B)** Reversibility of K+-induced ATP release. ATP was measured from the same oocytes before, immediately after the K^+ stimulus, and 20 or 40 minutes after replacement of the K^+ stimulus with regular oocyte Ringer solution (OR, wash). **(C)** ATP release from oocytes expressing Cx46 in the presence of oocyte Ringer solution (OR), or holding the membrane potential at 0 mV under voltage-clamp conditions in the presence or absence of CBX (200 μM). For all panels, data are shown as means ± SD. (N=5 for each measurement)

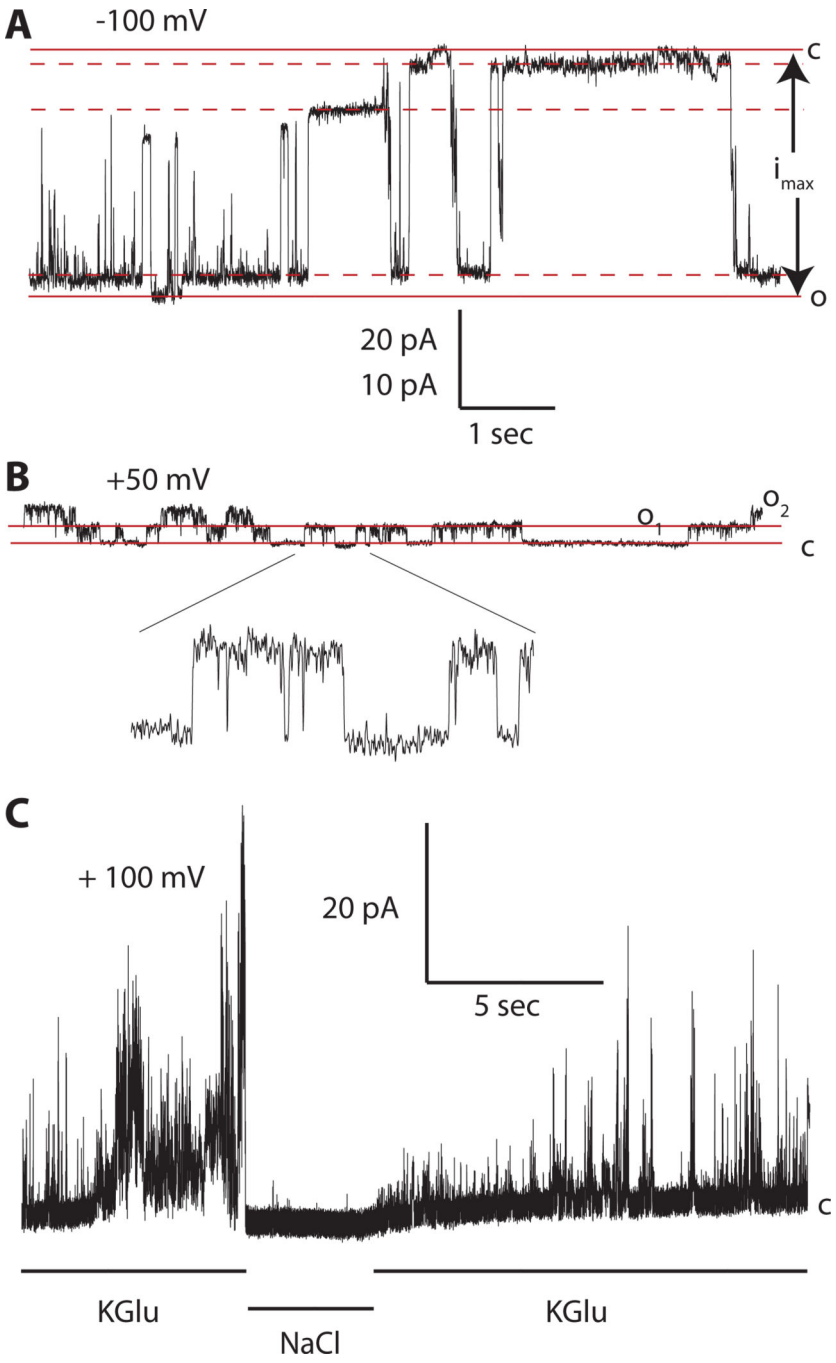

Fig. 3.

Single-channel recordings of Panx1 channels with K^+ or Na^+ in the extracellular solution. **(A)** An inside-out membrane patch exposed to high extracellular [K^+] and clamped at – 100 mV exhibited a maximal conductance of ~500 pS. The fully open and fully closed states are indicated by solid lines; the dashed lines indicate levels of three major subconductances. The current amplitude determined by the solid lines (i_{max}) was used to calculate the maximal conductance (g_{max}) of the Panx1 channels contained in different patches.

(B) An outside-out patch exposed to a low extracellular [K^+] (OR) and clamped at + 50 mV containing two channels that opened to the current levels O_1 and O_2. A segment of the record with single channel activity is shown at extended scale (5×) as indicated. The pA/sec scale applies to the main recordings in A (20 pA) and B (10 pA).
(C) Current record from an outside-out patch held at +100 mV and sequentially exposed to high K^+ solution (150 mM KGlu), normal OR (NaCl), and then high K^+ solution.

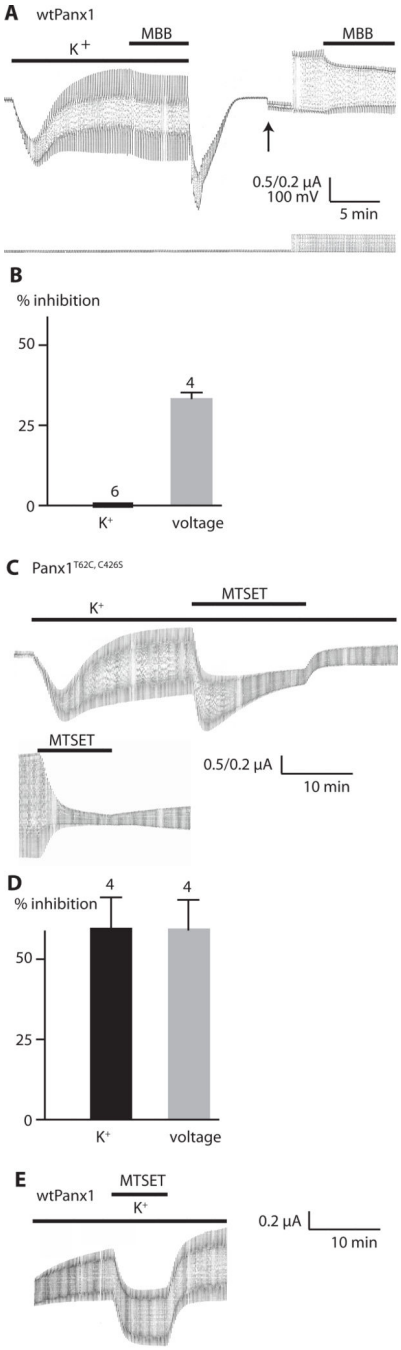

Fig. 4.

Modification by thiol reaction of Panx1 channels activated by K^+ or by voltage. **(A)** Current traces recorded from an oocyte expressing wild-type Panx1 (wtPanx1). The membrane potential was held at −50 mV and 5 mV voltage pulses were applied at a rate of 0.1 Hz. Lower bar indicates KGlu (85 mM, K^+); upper bar indicates presence of 100 µM MMB. KGlu and MMB were washed out and solution was replaced with oocyte Ringer solution, allowing, the membrane currents and conductance to return to baseline. After changing the gain (upward arrow), the pulse amplitude was increased to 100 mV (downward arrow) to

stimulate voltage-activated Panx1 channel currents. Bar indicates the presence of 100 μM MBB. **(B)** Quantitative analysis of current inhibition by MBB for K^+-activated and voltage-induced Panx1 channel currents. The number of measurements (N) is indicated above the bars. Data are shown as means ± SD. (**C**) Current traces from oocytes expressing $Panx1^{T62C,C426S}$ channels. Recording conditions were the same as in (A). Upper trace shows the effect of 1 mM MTSET on K^+-activated Panx1 current. Lower trace shows the effect on voltage-activated current. Because of the reactivity of the thiol groups in K^+ with MTSET, different oocytes were used for testing the effects on K^+-activated and voltage-activated Panx1 currents. (**D**) Quantitative analysis of current inhibition by 1 mM MTSET for K^+-activated and voltage-induced $Panx1^{T62C,C426S}$ channel currents. Data are shown as means ± SD. N is indicated above the bars. (**E**) Current traces of oocytes expressing wtPanx1. Recording conditions were the same as in (A). Panx1 was activated by K^+ as indicated, and MTSET (1 mM) was applied as shown by the bar.

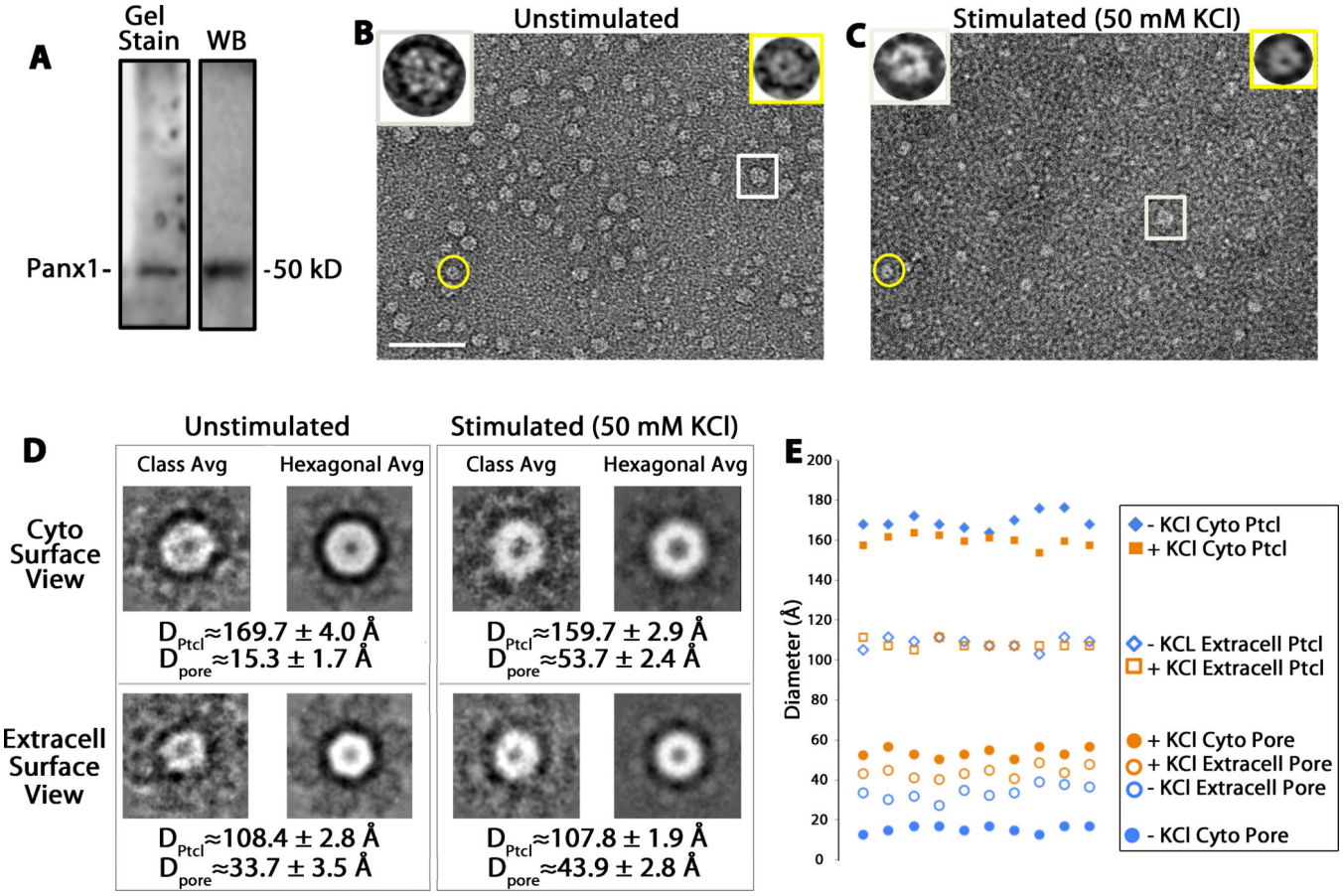

Fig. 5.

EM image analysis of negatively stained Panx1 oligomers. **(A)** Preparations purified from baculovirus-infected Sf9 cells as detected on a Sypro Ruby-stained protein gel (Gel Stain) and a corresponding Western Blot (WB). **(B, C)** Two representative low dose electron micrographs for uranyl acetate-stained purified Panx1 channels diluted in water (B, unstimulated condition) and in KCl 50 mM (C, stimulated condition). These micrographs were recorded with a standard low dose imaging protocol (47) to minimize electron beam damage and preserve higher resolution structural features. The scale bar represents 50 nm. The insets on the top of the micrographs are three-fold enlargements of the encircled particles. The rectangle indicates one channel with the cytoplasmic view of the Panx1 channel facing up, and the circle indicates a channel with the extracellular view facing up. **(D)** Representative class averages (Class Avg) and hexagonal-symmetrized averages (Hexagonal Avg) of cytoplasmic and extracellular surface views of unstimulated and stimulated Panx1 channels. Shown also are averages and standard deviations from 10 measurements of the channel and pore diameters of 4–5 class averages for both views from the two conditions. **(E)** Scatter plot of the measurements shown in (D, n=10 for each measurement). +/−KCl Cyto Ptcl, stimulated and unstimulated cytoplasmic particle outer diameter; +/− KCl Extracell Ptcl, stimulated and unstimulated extracellular particle outer diameter

Table 1

Appearance of large-conductance (500-pS) channel, ATP release, or dye uptake in response to various stimuli. CHO, Chinese hamster ovary; HEK 293, human embryonic kidney 293; nd, not determined.

Physiological stimulation of Panx1	**Large channel (~500 pS)**	**ATP release or dye uptake**	**cell type**	**references**
Mechanical stress	yes	yes	oocyte, erythrocyte	(1, 2)
Low oxygen	yes	yes	erythrocyte, neuron	(2, 20)
Intracellular Ca^{2+}	yes	yes	oocyte	(7)
ATP activating purinergic receptor signaling	nd	yes	oocyte	(7, 8)
Glutamate activating NMDA receptor signaling	nd	yes	neuron	(39)
Panx1 activated experimentally or under pathological condition				
Extracellular K^+	yes	yes	oocyte, erythrocyte, astrocyte	(1, 9, 12, 13, 30, 50)
Caspase 3 cleavage	nd	yes	Jurkat cells	(27)
Exclusively voltage-gated Panx1				
	no, 50–70 pS channel	no	HEK 293 cells, CHO cells, oocyte	(17, 18), present study